The Formation of Naphthalene, Azulene, and Fulvalene from Cyclic C_5 Species in Combustion: An Ab Initio/RRKM Study of 9-H-Fulvalenyl ($C_5H_5-C_5H_4$) Radical Rearrangements†

V. V. Kislov‡ and A. M. Mebel*

Department of Chemistry and Biochemistry, Florida International University, Miami, Florida 33199

Received: April 25, 2007; In Final Form: July 12, 2007

Chemically accurate ab initio Gaussian-3-type calculations of the $C_{10}H_9$ potential energy surface (PES) for rearrangements of the 9-H-fulvalenyl radical $C_5H_5-C_5H_4$ have been performed to investigate the formation mechanisms of polycyclic aromatic hydrocarbons (PAHs) originated from the recombination of two cyclopentadienyl radicals (*c*-C_5H_5) as well as from the intermolecular addition of cyclopentadienyl to cyclopentadiene (*c*-C_5H_6) under combustion and pyrolytic conditions. Statistical theory calculations have been applied to obtain high-pressure-limit thermal rate constants, followed by solving kinetic equations to evaluate relative product yields. At the high-pressure limit, naphthalene, fulvalene, and azulene have been shown as the reaction products in rearrangements of the 9-H-fulvalenyl radical, with relative yields depending on temperature. At low temperatures ($T < 1000$ K), naphthalene is predicted to be the major product (>50%), whereas at higher temperatures the naphthalene yield rapidly decreases and the formation of fulvalene becomes dominant. At $T > 1500$ K, naphthalene and azulene are only minor products accounting for less than 10% of the total yield. The reactions involving cyclopentadienyl radicals and cyclopentadiene have thus been shown to give only a small contribution to the naphthalene production on the $C_{10}H_9$ PES at medium and high combustion temperatures. The high yields of fulvalene at these conditions indicate that cyclopentadienyl radical and cyclopentadiene more likely represent significant sources of cyclopentafused PAHs, which are possible fullerene precursors. Our results agree well with a low-temperature cyclopentadiene pyrolysis data, where naphthalene has been identified as the major reaction product together with indene. Azulene has been found to be only a minor product in 9-H-fulvalenyl radical rearrangements, with branching ratios of less than 5% at all studied temperatures. The production of naphthalene at low combustion temperatures ($T < 1000$ K) is governed by the spiran mechanism originally suggested by Melius et al. At higher temperatures, the alternative C−C bond scission route, which proceeds via the formation of the *cis*-4-phenylbutadienyl radical, is competitive with the spiran pathway. The contributions of the previously suggested methylene walk pathway to the production of naphthalene have been calculated to be negligible at all studied temperatures.

1. Introduction

The potential role of small five-membered-ring hydrocarbons and their radicals in the growth of polycyclic aromatic hydrocarbons (PAHs) has been widely discussed by the combustion community in the past decade.[1] Various mechanisms have been suggested, and some of them have been thoroughly investigated by ab initio and density functional (DFT) methods. For instance, Miller and Melius[2,3] have shown on the basis of bond additivity-corrected fourth-order Møller−Plesset perturbation theory (BAC-MP4) calculations that the formation of benzene from recombination products of two propargyl (C_3H_3) radicals involves fulvalene as a crucial intermediate. The cyclopentadienyl *c*-C_5H_5 radical, which is abundant in combustion flames, has been shown to be a potential benzene precursor through the $CH_3 + C_5H_5$ reaction.[4] Another important mechanism addressed in the present study involves rearrangements of 9-H-fulvalenyl radical (9HFLR), originated from the recombination of two cyclopentadienyl radicals. This radical-promoted spiran mechanism leading to naphthalene was initially introduced by Melius and coworkers.[3] According to their BAC-MP2 calculations, 9HFLR rearranges to naphthalene with rather low barriers. For that reason, this reaction sequence has been considered an important contributor to the formation of naphthalene in combustion flames,[1,3,5−7] along with the commonly accepted hydrogen abstraction acetylene addition (HACA) mechanism.[8] A similar mechanism involving the rearrangement of a recombination product of indenyl with cyclopentadienyl has been suggested by Marinov et al. to account for the production of phenanthrene in *n*-butane and ethylene flames.[5,6] It is worth noting that Miller and Melius considered only those spiran rearrangements on the $C_{10}H_9$ potential energy surface (PES) that lead to naphthalene, not including some potentially important routes resulting in the formation of other abundant PAH species such as azulene and fulvalene. As follows from a recent B3LYP/6-31G* study of azulene-to-naphthalene rearrangements,[9] azulene can isomerize to naphthalene by a methylene walk mechanism. Therefore, the 9HFLR → azulene → naphthalene route may also contribute to the naphthalene production along with the spiran 9HFLR → naphthalene mechanism suggested by Melius et al. Recently, the reaction of cyclopentadienyl radical addition to cyclopentadiene was studied using B3LYP/6-31G** DFT calculations

† Part of the "Sheng Hsien Lin Festschrift".

* Author to whom correspondence should be addressed. E-mail: mebela@fiu.edu.

‡ Permanent address: Institute of Solution Chemistry of Russian Academy of Sciences, 1 Akademicheskaya St., Ivanovo, 153045 Russia.

10.1021/jp0732099 CCC: $37.00
Published on Web 08/21/2007

SCHEME 1: Notation of Carbon Atoms in the Reaction Products of 9HFLR Rearrangements.

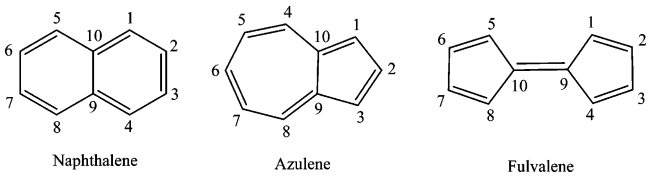

by Wang et al. to explain high yields of naphthalene, indene, and benzene in the cyclopentadiene pyrolysis.[10] They considered various rearrangements on the $C_{10}H_9$ and $C_{10}H_{11}$ PESs and also revisited the spiran pathway using DFT methods and suggested some additional routes leading to naphthalene on the $C_{10}H_9$ potential, for instance, the alternative C−C bond β-scission route. The spiran mechanism has been also recalculated by Alder et al. at the B3LYP/6-31G* level in their detailed DFT study of the azulene−naphthalene rearrangement.[9] The computed reaction barriers and energies for the spiran mechanism were found to be very similar to those obtained by Wang et al.,[10] but Alder and co-workers additionally considered other competitive routes, including C−C bond scission in the spiro radical leading to *cis*-4-phenylbutadienyl and rearrangement of the spiro radical to azulene, which can eventually lead to naphthalene through the methylene walk pathway. All 9HFLR−naphthalene rearrangements mentioned above exhibit barriers that are reasonably low for combustion conditions and therefore may contribute to the naphthalene formation in combustion flames. However, which mechanism of naphthalene formation on the $C_{10}H_9$ potential starting from the 9HFLR is the most important and what other possible reaction products exist in these rearrangements is not clear so far. To draw the most complete picture, a more detailed study of the $C_{10}H_9$ PES followed by statistical calculations of rate constants and product yields is required. Also, reaction energies more accurate than those from DFT calculations are very desirable.

In order to understand the role of five-membered-ring hydrocarbons in the formation of naphthalene and other PAH species, one needs to investigate the *c*-C_5H_5 + *c*-C_5H_5 and *c*-C_5H_5 + c-C_5H_6 reactions (the latter is more important in the pyrolysis of cyclopentadiene[10]) and, correspondingly, a variety of isomerization and dissociation processes on the $C_{10}H_{11}$, $C_{10}H_{10}$, $C_{10}H_9$, and $C_{10}H_8$ PESs. The $C_{10}H_8$ surface was carefully mapped out in our recent study where we considered the naphthalene−azulene rearrangements and their fragmentation pathways.[11] Calculations of the $C_{10}H_{11}$ and $C_{10}H_{10}$ PESs are currently ongoing in our group. In the present study, we concentrate only on the $C_{10}H_9$ surface and report ab initio Gaussian 3 (G3)-type calculations of the 9HFLR rearrangements leading to naphthalene, azulene, and fulvalene (shown in Scheme 1) followed by Rice−Ramsperger−Kassel−Marcus (RRKM) calculations of thermal reaction rate constants and relative product yields at the high-pressure limit. Our aim is to refine all known reaction routes at a much higher level of theory and to investigate other possible reaction pathways and products. The main goal is to assess the feasibility of various 9HFLR rearrangements leading to naphthalene, azulene, and fulvalene utilizing our accurate ab initio data in calculations of reaction rate constants and relative product yields.

2. Computational Methods

Geometries of all local minima and transition states were optimized using the hybrid density functional B3LYP[12] method with the 6-311G** basis set. Vibrational frequencies and molecular structural parameters obtained at the same level were utilized to calculate zero-point energy (ZPE) corrections, to characterize the stationary points, and to perform RRKM computations of reaction rate constants. Optimized Cartesian coordinates of all species involved in the reactions considered here are collected in Table S1 of the Supporting Information along with vibrational frequencies, ZPE corrections, B3LYP, RCCSD(T), MP2, and G3 total energies, and molecular structural parameters (moments of inertia and rotational constants).

To obtain accurate energies, we applied the G3(MP2,CC)//B3LYP modification[13] of the original G3 scheme[14] for high-level single-point energy calculations. The final energies at 0 K were obtained using the B3LYP optimized geometries and ZPE corrections according to the following formula:

$$E_0[\mathrm{G3(MP2,CC)}] = E[\mathrm{RCCSD(T)/6\text{-}311G(d,p)}] + \Delta E_{\mathrm{MP2}} + \Delta E(\mathrm{SO}) + E(\mathrm{HLC}) + E(\mathrm{ZPE})$$

where $\Delta E_{\mathrm{MP2}} = E[\mathrm{MP2/G3large}] - E[\mathrm{MP2/6\text{-}311G(d,p)}]$ is the basis set correction, ΔE(SO) is a spin−orbit correction (not included in our calculation), E(HLC) is a high-level correction, and E(ZPE) is the zero-point energy. The HLC was omitted in our calculation because, in most cases, the isomerizations of radical species considered here proceed without spin change, resulting in HLC cancellation. Otherwise, the neglect of HLC normally introduces an error of 2−3 kcal/mol. We tested the accuracy of this modified G3 scheme in our previous publications[15,16] and found a general agreement of 1−3 kcal/mol with available experimental barriers and reaction energies for the set of reactions relevant to the formation of PAH. For instance, the computed barriers and reaction energies of hydrogen abstraction from benzene and naphthalene by H and OH radicals, as well as acetylene addition to phenyl radical, agree with experimental parameters even better (within 0.5−1.0 kcal/mol).[15] The calculated heats of reaction for considered reactions relevant to the formation of indene[16] differ only by 1−3 kcal/mol from experimental values estimated using experimental enthalpies of formation. Generally, we found that this additive G3-type scheme is superior to the widely used G2/G2M schemes for the reactions relevant to the PAH formation. Here and below we, for brevity, denote the utilized G3-type scheme as G3. The computed barrier heights and heats of reaction for each individual reaction step, as well as the relative energies of all species involved in the formation and rearrangements of the 9HFLR, are shown in Figures 1 and 2. The B3LYP relative energies are collected for comparison in Table S1 of the Supporting Information. All DFT and MP2 calculations were carried out using the Gaussian 98[17] package, whereas the MOLPRO 2002[18] program package was used to calculate spin-restricted (R)/RCCSD(T) energies.

First-order thermal rate constants at the high-pressure limit were computed using the conventional RRKM theory.[19−21] For bimolecular reactions, such as hydrogen abstraction or hydrogen addition, we applied transition-state theory (TST)[22] to calculate second-order rate constants. Tunneling corrections to the rate constants were calculated using the simplest Wigner's formula[19] because, at combustion temperatures (>1000 K), tunneling does not play a significant role, and more sophisticated estimates for tunneling corrections are not necessary. All computed rate constants within the 300−3000 K temperature range are collected in Table S2 of the Supporting Information.

The fourth-order Runge−Kutta method with accuracy monitoring[23] was employed to solve the system of first-order,

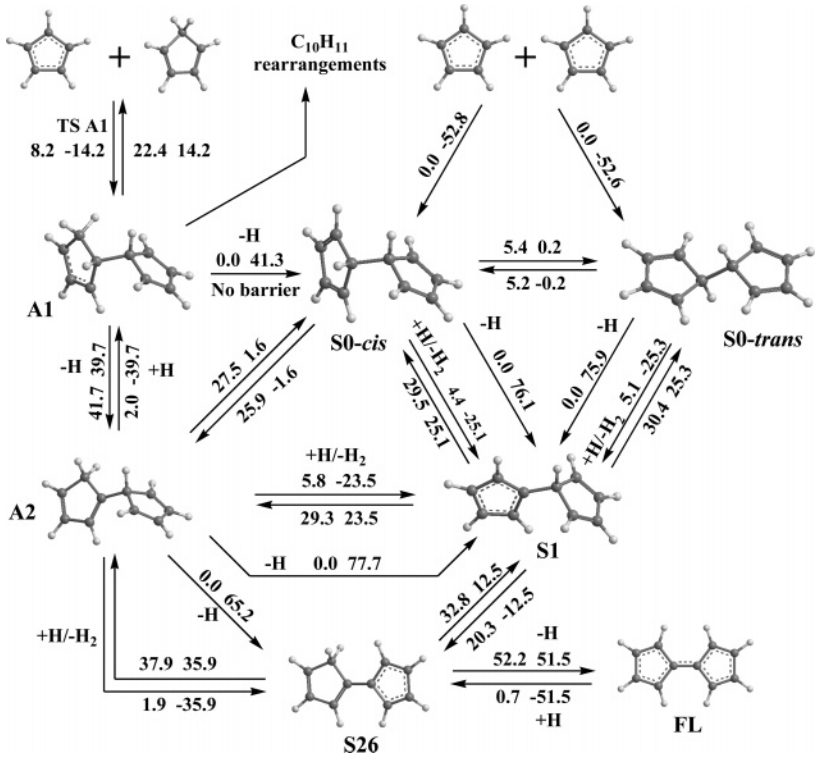

Figure 1. Formation pathways of 9HFLR (**S1**) involving the recombination of two cyclopentadienyl radicals *c*-C_5H_5 and the intermolecular addition of *c*-C_5H_5 to cyclopentadiene. The numbers show G3(MP2,CC)//B3LYP-computed barrier heights and heats of reaction.

phenomenological rate equations to obtain relative product yields (collected in Table 1).

3. Results and Discussion

A. Formation of 9HFLR at Combustion and Pyrolytic Conditions. Before discussing the PES for rearrangements of the 9HFLR, let us consider its possible formation mechanisms involving the cyclic C_5 species, the cyclopentadienyl radical, and cyclopentadiene. The suggested pathways are shown on Figure 1 along with G3-computed barrier heights and heats of reaction. The 9HFLR (**S1**) can be produced either by recombination of two cyclopentadienyl radicals leading to 9,10-dihydrofulvalene (**S0**) followed by abstraction or elimination of a hydrogen atom at the 9- or 10- positions, or as result of molecular−radical reactions between the cyclopentadienyl radical and cyclopentadiene. According to a recent photoionization mass spectrometry study of various fuel-rich flames (1,2-propadiene, propyne, cyclopentene, and benzene) coupled with electronic structure calculations, 1,3-cyclopentadiene and the cyclopentadienyl radical were found to be abundant, with 1,3-cyclopentadiene exhibiting significantly higher yields compared to the other, linear C_5H_6 species.[7] This indicates that the *c*-C_5H_5 + *c*-C_5H_6 reaction may be an important source of **S1** in combustion flames, in addition to the cyclopentadienyl radical self-recombination.

The cyclopentadienyl recombination is ∼53 kcal/mol exothermic and leads to the formation of **S0**, which has two conformers separated by a low barrier of ∼5 kcal/mol. Both conformers have nearly the same energies, with the trans isomer being slightly (by 0.2 kcal/mol) less stable than the cis structure. The strengths of C−H bonds at the 9- and 10- positions in **S0** are about 76 kcal/mol, and they can be cleaved at high temperatures to produce **S1**. Alternatively, abstraction of the hydrogen atoms sitting at the 9- and 10- positions (linked to sp3 carbons) exhibits low barriers (∼5 kcal/mol for both conformers), indicating that the **S1** can be formed from the recombination product of two cyclopentadienyl radicals by the abstraction mechanism in the presence of free H-radicals abundant in combustion flames. For comparison, according to our previous G3 calculations of the HACA mechanism,[15] H-abstraction from an sp2 carbon atom in benzene is endothermic by 8.8 kcal/mol and demonstrates a significantly higher barrier of 17.0 kcal/mol. A quantitative assessment of the role of the H elimination versus abstraction requires detailed kinetic modeling in real combustion conditions, and here we limit ourselves to the following qualitative consideration. At $T = 1500$ K, typical for combustion, the thermal energy distribution of **S0** will peak around 50 kcal/mol, as it is a large molecule. This means that, at the dissociation limit, activating collisions will be nearly as important as deactivating ones, and a large number of states populated at equilibrium will be unstable to dissociation of **S0** back to *c*-C_5H_5 + *c*-C_5H_5. As a result, stabilization of **S0** will be highly unlikely except at very high pressures. At the same time, the energy distribution of incipient complexes will also peak at ∼50 kcal/mol above the *c*-C_5H_5 + *c*-C_5H_5 limit, making it easier to overcome the 23 kcal/mol barrier to form **S1** + H. Consequently, the initial reaction should rather be written as *c*-C_5H_5 + *c*-C_5H_5 ⇆ **S1** + H via a short-living complex, and, since the complex is unstable, the H abstraction reaction is not probable.

The molecular−radical mechanism, which has been suggested as the only mechanism of naphthalene and indene formation in the cyclopentadiene pyrolysis,[10] appears to be more complicated. As seen in Figure 1, we considered several additional reaction pathways, which may be competitive. According to our G3 calculations, the intermolecular addition reaction of cyclopentadienyl radical *c*-C_5H_5 to the π bond of cyclopentadiene *c*-C_5H_6 exhibits a low barrier of 8.2 kcal/mol and is 14.2 kcal/mol exothermic, indicating that this molecular−radical mechanism is rather favorable energetically. The resonance-stabilized 1,9,10-

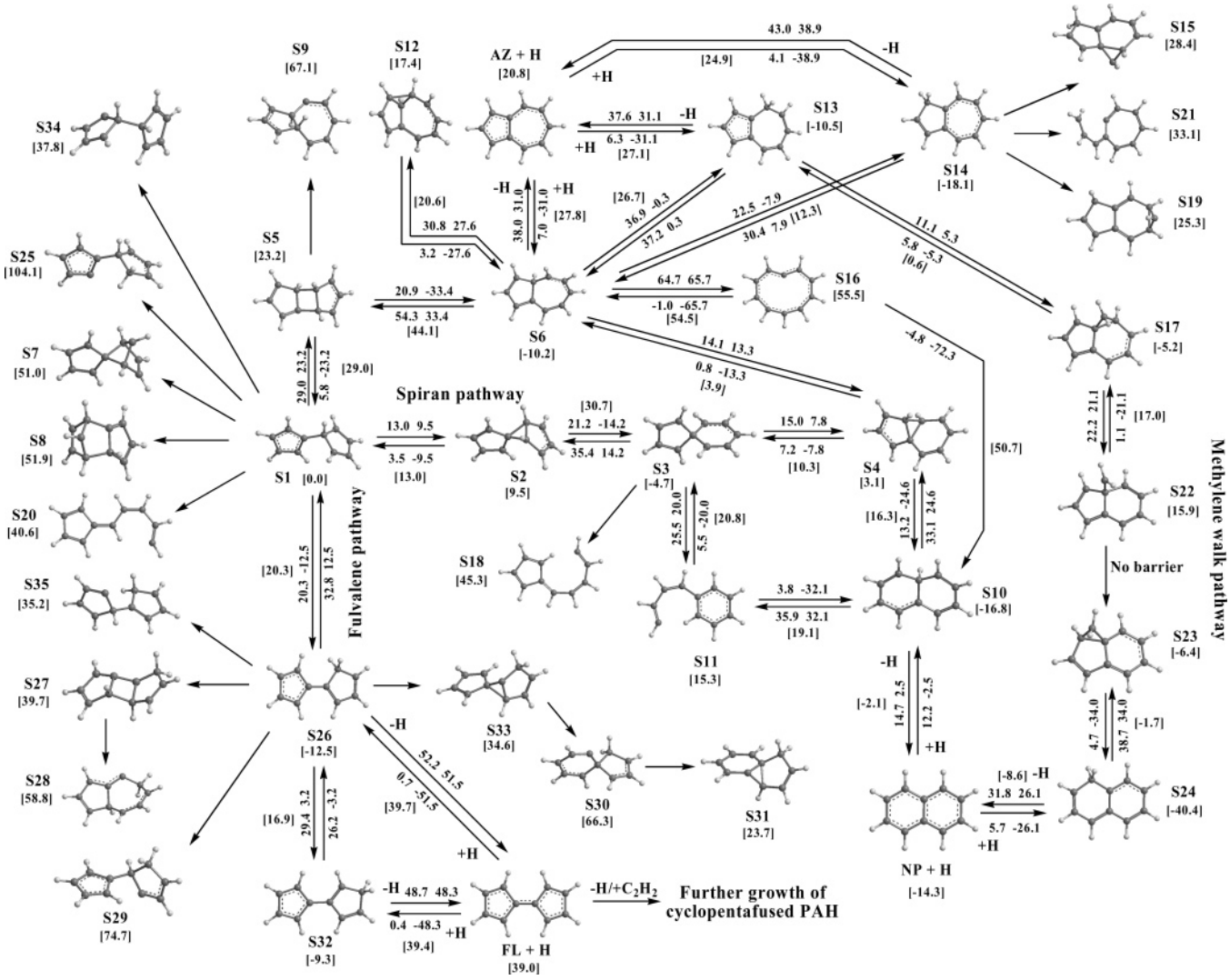

Figure 2. Rearrangements of 9HFLR (**S1**) leading to **NP**, **AZ**, and **FL**. The numbers show G3(MP2,CC)//B3LYP-computed barrier heights, heats of reaction, and energies relative to **S1** (in brackets).

TABLE 1: Calculated Product Yields (%) of NP, AZ, and FL from Rearrangements of 9HFLR

	total product yields			contributions to the total product yields from different pathways						
				NP tricyclic pathway	**NP** C−C bond scission	**NP** methylene	**AZ**	**AZ**	**AZ**	**NP** + **AZ**
T, K	**FL**	**NP**	**AZ**	(**S3** → **S4** → **S10** → **NP**)	(**S3** → **S11** → **S10** → **NP**)	walk	**S14** → **AZ**	**S6** → **AZ**	**S13** → **AZ**	(**S1** → **S5** → **S6**)
500	0.4	99.6	0.1	96.8	2.7	0.0	0.1	0.0	0.0	0.0
600	2.2	97.4	0.4	91.4	6.0	0.0	0.4	0.0	0.0	0.0
700	7.9	91.0	1.1	81.0	9.8	0.1	1.1	0.1	0.0	0.0
800	18.9	78.7	2.4	65.8	12.7	0.2	2.2	0.2	0.0	0.0
900	33.9	62.4	3.6	48.6	13.4	0.4	3.3	0.3	0.0	0.0
1000	49.4	46.1	4.5	33.3	12.3	0.4	4.0	0.5	0.0	0.1
1100	62.2	32.9	4.9	22.0	10.4	0.4	4.3	0.6	0.0	0.1
1200	72.0	23.2	4.8	14.4	8.4	0.4	4.1	0.6	0.0	0.1
1300	78.9	16.6	4.5	9.5	6.7	0.4	3.8	0.6	0.1	0.1
1400	83.8	12.1	4.1	6.4	5.4	0.3	3.4	0.6	0.1	0.1
1500	87.3	9.1	3.6	4.5	4.4	0.3	2.9	0.6	0.1	0.1
1700	91.6	5.6	2.8	2.4	3.1	0.2	2.2	0.5	0.1	0.1
1900	93.9	3.9	2.2	1.4	2.4	0.1	1.7	0.5	0.1	0.1
2000	94.6	3.4	2.0	1.2	2.1	0.1	1.4	0.5	0.1	0.1
2200	95.7	2.7	1.6	0.8	1.8	0.1	1.1	0.4	0.1	0.1
2400	96.3	2.3	1.4	0.6	1.6	0.1	0.9	0.4	0.1	0.2
2600	96.8	2.0	1.2	0.5	1.5	0.0	0.7	0.4	0.1	0.2
2800	97.0	1.9	1.1	0.5	1.4	0.0	0.6	0.4	0.1	0.2
3000	97.2	1.8	1.0	0.4	1.3	0.0	0.6	0.4	0.1	0.2

trihydrofulvalenyl radical (**A1**) adduct formed at the first step further undergoes H-elimination, producing either **S0** or 1,10-dihydrofulvalene (**A2**). The former H-elimination step does not have an exit barrier (this was confirmed by a PES scan) and requires 41.3 kcal/mol of internal energy to eliminate the hydrogen atom. The alternative H-elimination at the 10- position exhibits a barrier of 41.7 kcal/mol and is endothermic by 39.7 kcal/mol. Both steps seem to be competitive and should be taken

into account. **S1** can be obtained from the **S0** and **A2** species by hydrogen elimination or abstraction reactions; the latter exhibits low barriers of 4.4 kcal/mol and 5.8 kcal/mol for the **S0** + H → **S1** + H_2 and **A2** + H → **S1** + H_2 steps, respectively. **A2** may also rearrange to **S0** through the 1,9 H-shift reaction **A2** → **S0**, overcoming a barrier of 27.5 kcal/mol. Another possibility involves H-elimination or abstraction at the 10-position in **A2**, leading to the 1-H-fulvalenyl radical **S26** (which turns out to be an important fulvalene precursor on the $C_{10}H_9$ PES; see below), which then rearranges to **S1** by the 1,9 H-migration. As will be shown below in Section 3.C, at medium and high temperatures, the fate of the **S26** radical is to produce fulvalene (**FL**). Therefore, at those conditions, the **A1** → **A2** → **S26** reaction channel should be considered as a **FL** formation pathway instead of a means of producing **S1**. However, at low reaction temperatures (e.g., in the case of low-temperature pyrolysis of cyclopentadiene), the contribution of the **A1** → **A2** → **S26** → **S1** mechanism to the formation of 9-H-fulvalenyl may be significant.

Another issue, which is not addressed in the present study, concerns various rearrangements on the $C_{10}H_{11}$ PES involving, for example, the **A1** radical. Indeed, this intermediate may take part in further rearrangements, instead of undergoing the previously considered **A1** → **A2** + H and **A1** → **S0** + H hydrogen elimination steps, which require more than 40 kcal/mol of internal energy for the H loss. In principle, naphthalene, azulene, or other PAHs (e.g., indene[10]) may be formed as a result of such rearrangements on the $C_{10}H_{11}$ surface.

B. PES for Unimolecular Rearrangements of S1. Figure 2 depicts all rearrangements of **S1** explored in this study, along with G3-computed barrier heights, reaction energies, and G3 relative energies (in brackets) of intermediates and transition states with respect to **S1**. We tried to map out all possible rearrangements of **S1**, which have reasonably low barriers with regard to combustion conditions. For a variety of intermediates (**S7**−**S9**, **S15**, **S18**−**S21**, **S25**, **S27**−**S31**, and **S33**−**S35**) with high relative energies, we have omitted a detailed investigation of transition states for their formation and further transformations because they are hardly competitive with the major C_5H_5−C_5H_4 transformation routes in combustion. The major reaction products of **S1** rearrangements appeared to be naphthalene (**NP**), azulene (**AZ**), and fulvalene (**FL**). Let us further discuss all considered pathways in more detail.

After being formed, the **S1** radical can rearrange by three most energetically favorable pathways. The first one is the so-called spiran mechanism passing through the formation of the C_{2v}-symmetric spiro adduct **S3** to the tricyclyl radical **S4**, which then undergoes ring opening, producing either the 9-H-naphthyl radical (**S10**) with a barrier of 13.2 kcal/mol, or, more likely, the 9-H-azulyl radical (**S6**) with a barrier height of only 0.8 kcal/mol. **S10** and **S6** can lose an "extra" hydrogen atom, producing **NP** and **AZ**, respectively. The spiran pathway leading to **NP** (**S1** → **S2** → **S3** → **S4** → **S10** → **NP**) was initially suggested and investigated by Melius et al.[3] at the BAC-MP2 level, whereas the rearrangement of the **S4** adduct leading to **AZ** was studied recently by Alder et al.[9] at the B3LYP/6-31G* level along with a variety of **AZ**-to-**NP** isomerization pathways. The second **S1** radical rearrangement, **S1** → **S5** → **S6**, involves the formation of the tricyclic intermediate **S5** with two five-membered and one four-membered ring. After the ring opening, which is 33.4 kcal/mol exothermic, the **S5** adduct rearranges to the 10-H-azulyl radical (**S6**), a precursor of **AZ**. Whereas the first two pathways lead to **NP** or **AZ** and are interconnected at the **S6** intermediate, the third route, **S1** → **S26** → **S32** → **FL**, proceeds to another product, **FL**, through two consecutive H-atom migrations, 9,1- H-migration producing the **S26** radical, followed by 1,2- H-atom shift leading to 2-H-fulvalenyl **S32**, which then undergoes H-elimination, producing **FL**. **FL** is not likely to be a precursor of **NP** or **AZ** on the $C_{10}H_9$ PES but may further be involved in H-abstraction/C_2H_2-addition sequences, giving rise to a variety of cyclopentafused PAHs, which are the possible fullerene precursors.[24,25] The pathways leading to the **S6** adduct via the **S5** tricyclic intermediate and the **FL** pathway were not considered in previous theoretical studies, although the spiran mechanism was thoroughly investigated by the DFT method. As follows from the reaction scheme shown in Figure 2, all three **S1** rearrangement pathways exhibit low barriers regarding the combustion conditions and therefore should be competitive.

The spiran pathway starts with the three-membered-ring closure **S1** → **S2**, endothermic by 9.5 kcal/mol and producing a metastable tricyclic intermediate **S2**, which then rearranges to the more stable C_{2v}-symmetric spiro adduct **S3** by ring expansion. The reverse barrier for the **S1** → **S2** ring closure is only 3.5 kcal/mol, much lower than the forward barrier of 13 kcal/mol, and that for the subsequent ring expansion **S2** → **S3** is 21.2 kcal/mol. Therefore, the equilibrium of the **S1** → **S2** reaction should be shifted toward the initial reactant, and one has to consider the overall barrier of 30.7 kcal/mol for the **S1** → **S2** → **S3** rearrangement. From this point of view, the **S1** → **S5** and **S1** → **S26** reactions appear to be strong competitors with the spiran pathway in spite of the fact that both of them exhibit higher barriers than that for the **S1** → **S2** ring closure. The **S3** bicyclic adduct can then either rearrange to the tricyclic intermediate **S4** by three-membered-ring closure or undergo a C−C bond scission leading to the opening of the five-membered ring and producing *cis*-4-phenylbutadienyl (**S11**). The latter reaction is less favorable energetically because it exhibits a barrier about 10 kcal/mol higher than that for the **S3** → **S4** three-membered-ring closure, and is also ∼20 kcal/mol endothermic. Therefore, the C−C bond scission pathway **S3** → **S11** → **S10** → **NP** is expected to give only a minor contribution to the production of **NP**, whereas the **S3** → **S4** rearrangement controls the spiran mechanism, eventually leading to either **NP** or **AZ** after the formation of the tricyclyl radical **S4**. Interestingly, both **S1** → **S2** and **S3** → **S4** three-membered-ring closure reactions exhibit very similar barriers of 13.0 and 15.0 kcal/mol and reaction endothermicities of 9.5 and 7.8 kcal/mol, respectively. Although the **S3** → **S11** C−C bond scission is not favorable energetically, the subsequent six-membered-ring closure **S11** → **S10** easily transforms **S11** to **S10** with a barrier of only 3.8 kcal/mol. **S10** is a **NP** precursor that proceeds to **NP** by a one-step elimination of an "extra" hydrogen atom. We also considered the alternative C−C bond scission leading to the opening of the six-membered ring, **S3** → **S18**, and found that this process is unlikely at typical combustion temperatures. Indeed, the **S3** → **S18** reaction is computed to be 50 kcal/mol endothermic, indicating that the corresponding barrier is expected to be even higher, and therefore this process should not be competitive with the **S3** → **S4** or **S3** → **S11** rearrangements at the conditions relevant to combustion.

At this stage, the **S1** → **S2** → **S3** → **S4** sequence appears to be the dominant route within the spiran pathway. After **S4** is formed, the reaction sequence is branched, leading to two different products, either **NP** or **AZ**. The expansion of the five-membered ring in **S4** (**S4** → **S10**) leads to the formation of **S10** (an **NP** precursor) with a barrier of 13.2 kcal/mol, whereas the expansion of the six-membered ring (**S4** → **S6**) produces **S6**

(an **AZ** precursor) over a very small barrier of 0.8 kcal/mol. One can see that the **S4** → **S6** six-membered-ring expansion is significantly more favorable energetically than the **S4** → **S10** five-membered-ring expansion. From this point of view, it seems that the **S4** → **S10** → **NP** route is hardly competitive with the **S4** → **S6** → **AZ** pathway, and that **NP** should be considered only as a minor product of the spiran rearrangement. However, this is not the case because one has to take into account the barriers for further transformations of **S6**. Indeed, the **AZ** formation from **S6** by H-elimination requires a high activation energy of 38 kcal/mol. The other rearrangements of the **S6** adduct, **S6** → **S13**, **S6** → **S14**, and **S6** → **S12**, also demonstrate rather high barriers (36.9, 22.5, and 30.8 kcal/mol, respectively) as compared to the contesting **S6** → **S4** reverse step, which has a barrier of only 14.1 kcal/mol. In this situation, the **S4** → **S10** rearrangement can give a considerable contribution to the formation of **S10** and, eventually, to the production of **NP**. In the subsequent section, we discuss this issue in more detail considering the computed rate and equilibrium constants as well as the relative product yields.

S6, which is 13.3 and 10.2 kcal/mol more stable than the **S4** intermediate and the initial **S1** radical, respectively, is an obvious precursor of **AZ**. The **AZ** molecule can be obtained either by direct elimination of an "extra" hydrogen atom from **S6** with a barrier of 38 kcal/mol or by prior H-migrations producing 4-H-azulyl (**S13**) or 1-H-azulyl (**S14**) radicals followed by subsequent H-eliminations. The formation of **S14**, the most stable intermediate within the spiran mechanism, appears to be the most energetically favorable process among these three reactions because it has a barrier of only 22.5 kcal/mol, whereas the other transformations of **S6** exhibit much higher barriers, normally above 30 kcal/mol. On the other hand, the H-elimination from **S14** has a higher barrier of 43 kcal/mol as compared to the respective H-eliminations from **S6** and **S13**. **S13** may further be involved in the methylene walk rearrangement, **S13** → **S17** → **S22** → **S23** → **S24** → **NP**, instead of the H-elimination process **S13** → **AZ** because the 11.1 kcal/mol barrier for the **S13** → **S17** three-membered-ring closure reaction is significantly lower than the 38 kcal/mol barrier for the H-elimination from **S13**. Keeping this in mind, we consider that the most probable **AZ** production reactions are the direct H-elimination from **S6** and the **S6** → **S14** → **AZ** sequence. The formation of the **S13** intermediate by the **S6** → **S13** H-migration acts as a sink of the **S6** adduct, promoting the production of **NP** through the competitive methylene walk mechanism. In principle, **S14** may undergo alternative rearrangements competing with the H-atom elimination **S14** → **AZ**, which require higher activation energies of at least 43 kcal/mol. For instance, the 7,10- or 5,7- three-membered-ring closure reactions produce isomers **S15** and **S19**, respectively, and the 1,9 C−C bond scission in the five-membered ring leads to the **S21** radical. Taking into account the relative energies of **S15**, **S21**, and **S19** with respect to **S14**, all these steps are expected to have barriers higher than 43 kcal/mol, but they may be comparable to the reaction barrier for the H-atom elimination from **S14**. However, further rearrangements of these intermediates are not relevant to the formation of any stable PAH molecules, such as **NP**, **AZ**, or even indene, and hence we excluded them from the present consideration.

We have also investigated two additional rearrangements of **S6**, which are hardly competitive with the previously discussed reactions consuming this intermediate. The first route involves 9,10- bond cleavage in **S6**, producing the C_{2v}-symmetric monocyclic radical intermediate **S16** with a high barrier of 64.7 kcal/mol. This reaction is also highly endothermic. At the B3LYP/6-311G** level, the reverse barrier was found to be 9.7 kcal/mol; however, it disappears at the G3 level, at which the energy of the transition state is 1 kcal/mol lower than that of **S16**. The barrier for the 9,10-ring closure in **S16** leading to **S10**, which is positive at the B3LYP/6-311G** level (5.1 kcal/mol), also becomes negative (−4.8 kcal/mol) at the G3 level. We suppose that the **S16** intermediate, if it exists, can be only a very shallow local minima on the $C_{10}H_9$ PES with respect to the transition states for **S6** → **S16** and **S16** → **S10**. The B3LYP method apparently overestimates the barrier heights for these reactions. A similar mechanism on the $C_{10}H_7$ PES passing through the 9,10- bond cleavage in the 4-azulenyl radical followed by the formation of the 1-naphthalenyl radical was considered by Alder et al.[9] in their B3LYP study of the **AZ**−**NP** rearrangement. The B3LYP/6-31G* computed barrier for the 9,10- bond cleavage in the 4-azulenyl radical was found to be 38 kcal/mol, which is significantly lower than the barrier for the 9,10- bond cleavage in **S6**. Therefore, such a mechanism may contribute to the **NP** production on the $C_{10}H_7$ PES, but is not likely to be competitive on the $C_{10}H_9$ PES where the **S6** → **S16** isomerization requires 64.5 kcal/mol of activation energy. Another rearrangement of **S6**, which is not relevant to the production of **NP** or **AZ**, is the formation of the tricyclic intermediate **S12** via a 1,4-ring closure. This reaction has a barrier of 30.8 kcal/mol and, in principle, can compete with other transformation routes of **S6**. However, the **S12** radical is most likely to be a dead end on the surface because its further possible transformations through 1,9-, 9,10- or 4,9- bond-scission reactions are expected to have high barriers and therefore would hardly be competitive with the **S12** → **S6** reverse step, which exhibits a low barrier of 3.2 kcal/mol. Thus, we expect that the **S6** adduct is not consumed by the **S6** → **S12** rearrangement, but rather is involved in the **S6** → **AZ**, **S6** → **S13**, and **S6** → **S14** transformations.

The methylene walk pathway was suggested by Alder et al.[9] to explain the thermal rearrangement of **AZ** to **NP**, which takes place at temperatures above 400 °C. The B3LYP/6-31G* calculations[9] have shown this radical-promoted mechanism to exhibit low barriers, and therefore it can account for the production of **NP** both in thermolysis and in combustion, together with the spiran mechanism. The methylene walk pathway, **S13** → **S17** → **S22** → **S23** → **S24** → **NP**, starts from the formation of **S13**; the creation of a CH_2 group is required for the subsequent 5,9-closure of a three-membered ring. This mechanism acts as an **AZ** sink, converting a certain amount of **AZ** or its precursors (**S6** and **S13** in our case) to **NP**. In other words, the methylene walk pathway competes with the spiran mechanism, providing a higher yield of **NP**. We recomputed all the structures obtained previously[9] for the methylene walk pathway at the higher B3LYP/6-311G** level and refined their energies at the G3 level. For all B3LYP-computed geometries and relative energies, we obtained good agreement with the previous results by Alder et al.[9] The only exception is the transition state for methylene transfer from the six-membered ring in 4,9-cyclopropylyl (**S17**) to the five-membered ring to form 1,9-cyclopropylyl (**S23**). According to their B3LYP/6-31G* calculations, the 9-methylyl radical (**S22**) was identified as a transition state with one imaginary frequency of 190*i*, which interconnects the **S17** and **S23** intermediates. We tested their reported structure of **S22** with intrinsic reaction coordinate (IRC) calculation and found that it represents a transition state for a degenerate rotation of the CH_2 fragment around the adjoining C−C bond, but not a transition state for the interconversion of **S17** to **S23**. Moreover, at the B3LYP/6-311G** level, we were

able to obtain a local minimum structure for **S22**; it has a slightly different orientation of the CH_2 fragment compared to the structure reported by Alder et al. A further search of an **S22** → **S23** ring-closure transition state was unsuccessful, and a careful scan of the PES in this vicinity showed that this reaction is essentially barrierless. We suppose that **S22** corresponds to a shallow local minimum on the PES with regard to a **S22** → **S23** transition state, and hence this transition state is very difficult to locate. For the purpose of rate constant calculations, we suggest that the transition state for ring opening, **S17** → **S22**, can be treated as the transition state for interconversion between **S17** and **S23**.

All considered steps within the methylene walk pathway exhibit quite low barrier heights at the G3 level, indicating that this mechanism is highly competitive. Indeed, the initial 5,9-three-membered-ring closure producing **S17** has a barrier of only 11.1 kcal/mol, which is significantly lower than the competing H-elimination **S13** → **AZ** process leading to **AZ** and exhibiting a barrier of 37.6 kcal/mol, or the rearrangement of **S13** back to **S6** with a barrier of 37.2 kcal/mol. Such a large difference in reaction barriers indicates that, once formed, the **S13** adduct mostly rearranges to **NP** by the methylene walk pathway. The highest barrier of 22.2 kcal/mol within the methylene walk pathway is calculated for the interconversion of **S17** to **S23**. After that, the **S23** intermediate easily rearranges to 1-H-naphthyl **S24** (the most stable radical within the considered $C_{10}H_9$ PES) over a barrier of only 4.7 kcal/mol. The **S23** → **S24** reaction is 34 kcal/mol exothermic. Finally, **NP** can be obtained by H-atom elimination from **S24**.

In the present study we also found an additional competitive rearrangement pathway of **S1** proceeding through the formation of the tricyclic intermediate **S5** to **S6**, which then transforms to **AZ** or **NP** as discussed above. The route starts from the 4,8-ring closure of a four-membered ring, **S1** → **S5**, with a barrier of 29 kcal/mol. The moderate barrier height indicates that this reaction may compete with the other rearrangements of **S1** considered here. However, the subsequent 7,8- ring expansion in **S5** requires 20.9 kcal/mol of activation energy, which is almost four times higher than the contending reverse **S5** → **S1** step with a barrier of only 5.8 kcal/mol. Hence, we expect the **S1** → **S5** → **S6** route to give only a minor contribution to the total **AZ**/**NP** yields as compared to the spiran pathway. In the following section, we discuss this issue in more detail. The alternative 9,10- ring expansion in **S5** leading to the triradical intermediate **S9** is hardly competitive with the 7,8- ring expansion because the former process is expected to have a barrier higher than 44 kcal/mol. Therefore, we conclude that the **S5** → **S9** reaction is not relevant to the production of **AZ** or **NP** within the studied network.

Now let us discuss the most energetically favorable **S1** → **S26** → **S32** → **FL** rearrangement of the **S1** radical leading to the formation of **FL**. This route was not considered previously, but our calculations show it to be a major pathway for rearrangements of **S1**. The pathway involves three steps: the 9,1- hydrogen-atom migration producing **S26** with a barrier of 20.3 kcal/mol followed by a 1,2- hydrogen atom shift with a barrier of 29.4 kcal/mol leading to **S32**, and in the final step, **S32** undergoes H-atom elimination from the CH_2 group producing **FL** with a relatively high barrier of 48.7 kcal/mol. **S26** is 12.5 kcal/mol more stable than **S1**, hence, the initial hydrogen shift reaction is exothermic. The barrier for this reaction is almost 10 kcal/mol lower than that for the competing **S1** → **S5** reaction and also 10.4 kcal/mol lower than the effective barrier for the **S1** → **S2** → **S3** rearrangement (see the discussion on the spiran mechanism above). Therefore, the **FL** mechanism is likely to be the major **S1** consumption route, meaning that **FL** is expected to be the major reaction product within the considered network. It will be shown below that the **FL** route accounts for >50% of the **S1** consumption at $T > 1000$ K. **S26** may undergo a direct H-atom elimination (**S26** → **FL**), producing **FL** with a barrier of 52.2 kcal/mol, which is close to the barrier of 48.7 kcal/mol for the H-elimination from **S32**. However, the direct **S26** → **FL** channel is hardly competitive with the **S26** → **S32** hydrogen migration, which is prior to the subsequent H loss from the **S32** radical. This follows from a comparison of respective barriers: the barrier for **S26** → **S32** isomerization (29.4 kcal/mol) is 22.8 kcal/mol lower than the 52.2 kcal/mol barrier for the direct H loss from **S26**. This indicates that the formation of **FL** proceeds via a prior isomerization of **S26** to the **S32** radical, and then the latter undergoes H-atom loss, which is significantly faster than the H loss from **S26** (the comparison of rate constants will be given in the subsequent section).

SCHEME 2: Most Probable Cyclopentafused PAHs Originated from FL.

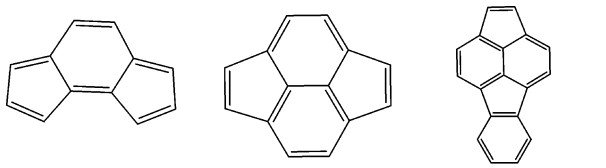

Because the H eliminations from very stable **S26** and **S32** radicals exhibit rather high barriers (~50 kcal/mol), we investigated other possible rearrangements of **S26**, which are expected to compete with the considered H-migration and H-loss reactions. The **S26** → **S33** → **S30** → **S31** route is similar to the spiran pathway, but it involves the formation of energetically high-lying isomers, especially the triradical intermediate **S30**. From this point of view, this pathway requires very high activation energies and therefore is hardly competitive. The formation of the tricyclic radical **S27**, which is akin to **S5**, may be a viable alternative, but the further rearrangement of **S27** involves highly energetically unfavorable ring expansion, leading to the triradical structure **S28**. The 4,9- hydrogen-atom shift within the **S26** radical can produce the triradical structure **S29**, but the corresponding barrier is expected to be higher than 70 kcal/mol. All this makes the other transformations of **S26** unlikely at the combustion conditions and not relevant to the production of **NP** or **AZ**. **FL** can be considered as an important precursor for a variety of cyclopentafused PAHs,[24,25] especially those relevant to the formation of bowl-shaped PAHs, fullerenes, and fullerenic nanostructures. For example, the 1-H abstraction from **FL** followed by subsequent acetylene addition and ring closure can lead to the formation of indacene ($C_{12}H_8$) at the first stage, and the addition of another acetylene produces pyracylene ($C_{14}H_8$), and so on (see Scheme 2).

As was mentioned above, we excluded from our consideration several isomerization pathways of **S1** involving the formation of unstable and energetically high-lying radicals **S7**, **S8**, **S20**, **S34**, and triradical **S25** because they are not competitive with the discussed rearrangements of **S1** at combustion conditions and ultimately are not relevant to the formation of PAHs addressed in this study. Theoretically, the 5,9- bond scission, **S1** → **S20**, may lead to **S6** if followed by closure of the seven-membered ring. However, the barrier for the **S1** → **S20** bond scission process is expected to be higher than 40 kcal/mol, and this value is significantly higher than the barriers for the other

contending **S1** transformations. Another issue is that the **S20** isomer, which has a planar C_s-symmetric structure, has to change its conformation prior to the seven-membered-ring closure. This process passes through an out-of-plane configuration of the **S20** radical. According to our calculations, during geometry optimization starting from an out-of-plane configuration, the **S20** radical undergoes the five-membered-ring closure and returns to the initial **S1** structure with no barrier; all attempts of geometry optimization of nonplanar structures in the vicinity of **S20** converged to **S1**. Therefore, the 5,9- bond scission **S1** → **S20** reaction is also unlikely to be a viable competitor among the considered isomerizations of **S1**. In the following section, on the basis of the statistical calculations of reaction rate constants, we discuss relative product yields in rearrangements of **S1**.

C. Relative Product Yields. Utilizing the RRKM-computed high-pressure-limit thermal rate constants collected in Table S2 of the Supporting Information, we performed calculations of relative yields of **NP**, **AZ**, and **FL** at infinite time by solving the kinetic equations for rearrangements of **S1**, including all unimolecular reaction steps. Considering that B3LYP/6-311G** frequencies and chemically accurate barriers and reaction energies computed at the G3 level were utilized in the RRKM calculations, we expect that the resulting thermal rate constants are of high accuracy, as long as the high-pressure limit adequately describes the reaction conditions. The calculated total product yields are collected in Table 1, along with contributions of different pathways to these yields.

At low temperature conditions (∼700−900 K), the major reaction product is **NP**, followed by **FL** and **AZ**. Starting from 1000 K (∼700 °C), where the **NP** and **FL** yields are similar, a further temperature increase promotes the **FL** production, which then becomes the major reaction product. At $T > 1500$ K, **NP** becomes only a minor product, accounting for less than 10% of the total product yield, along with **AZ**. The **AZ** production reaches its maximum value of 4.8% at 1200 K and is below 5% at all studied temperatures. This indicates that **AZ** is a minor product of **S1** rearrangements. Our results can explain the high **NP** production in the cyclopentadiene pyrolysis,[10,26] where **NP** and indene were identified as the major reaction products. Indeed, at the pyrolytic conditions in a laminar flow reactor, the temperatures of the cyclopentadiene pyrolysis were within 700−850 °C or 1000−1150 K. As follows from our calculations, **NP** yields are high in this temperature range. Interestingly, **FL**, which is a structural isomer of **NP**, was not identified by the gas chromatography−mass spectrometry technique among the products of the cyclopentadiene pyrolysis,[10,26] but another major detected product was indene. However, the formation of indene at the pyrolytic conditions most likely involves the radical−molecule reaction between cyclopentadienyl and cyclopentadiene leading to the **A1** adduct (see Figure 1) followed by further rearrangements to indene on the $C_{10}H_{11}$ PES.[10] This mechanism is not relevant to the rearrangements of **S1**, which take place on the $C_{10}H_9$ PES considered here. In flame combustion, the concentration of cyclopentadienyl radicals is high because they can be produced by the oxidation of phenyl radical with O_2.[27,28] The major source of **S1** at these conditions should arise from *c*-C_5H_5 self-recombination by the mechanism described above, and further transformations mostly take place on the $C_{10}H_9$ PES, prohibiting the formation of indene. The production of **NP** from **S1** in flame combustion is expected to be significant only at low temperatures or in low-temperature flame zones. At higher temperatures, the **NP** production is predicted to become negligible, giving way to the production of **FL** and, as a consequence, to higher cyclopentafused PAHs, which are potential precursors of fullerenes and fullerene-containing soot. We suppose that, at high combustion temperatures, where the concentration of H radicals is expected to be large, the **NP** formation is mostly governed by the conventional HACA mechanism.

The analysis of rate constants for the **S1** → **S2** and **S1** → **S26** reactions collected in Table 2 shows that, at 700 K, the former reaction is 23 times faster than the latter, and therefore the first step of the spiran sequence is more favorable than the competitive **S1** → **S26** hydrogen atom shift, which starts the reaction sequence leading to **FL**. The spiran sequence is more kinetically favorable, even though the equilibrium of the **S1** → **S2** reaction is shifted toward the reactant at these conditions. Then, with increasing temperature, the k(**S1** → **S2**)/k(**S1** → **S26**) ratio rapidly decreases, and, at 1500 K, both reactions have similar rates. On the other hand, the k(**S1** → **S26**)/k(**S2** → **S3**) ratio does not change significantly and remains within 2.7−1.5, indicating that both **S1** → **S26** and **S2** → **S3** reactions have comparable reaction rates, especially at medium and high temperatures. Taking into account that the equilibrium constant for the **S1** → **S2** reaction is less than 10^{-2} even at high temperatures, but K_{eq}(**S1** → **S26**) is always higher than 1, the **S1** → **S26** H-shift reaction starts to dominate at $T \sim 1000$ K. At higher temperatures, these trends dramatically increase, especially when k(**S1** → **S2**)/k(**S1** → **S26**) drops below 1.0, and the **S1** → **S26** → **S32** → **FL** route becomes the major **S1** consumption pathway, accounting for more than 90% of the total product yield at $T > 1500$ K. In principle, the **S26** adduct may undergo H-atom loss and produce **FL** directly, without prior isomerization to the **S32** radical. However, if we compare rate constants for the **S26** → **S32** and **S26** → **FL** reactions (see Table 2), it is clear that the latter step is not competitive because, at typical combustion temperatures, its rate constants have several orders of magnitude lower values than those for the **S26** → **S32** isomerization. Even at $T = 2000$ K, the **S26** → **S32** hydrogen migration is still more than 10 times faster than the **S26** → **FL** hydrogen atom loss. Additionally, the hydrogen atom elimination from the **S32** radical demonstrates significantly higher rates (3.8−2.8 times within the 1500−2000 K range) than those of the similar **S26** → **FL** reaction, although the barriers for both reactions are very close to each other (∼3 kcal/mol). Therefore, we assume that the **S1** → **S26** → **S32** → **FL** reaction is the major **FL** production channel, and the contribution of the **S26** → **FL** reaction should be negligible.

The calculated **AZ** product yields indicate that **AZ** is only a minor product in rearrangements of **S1** and, in particular, within the spiran mechanism. Hence, the cyclopentadienyl self-recombination is hardly a significant source of **AZ** in combustion flames. In contrast, **NP** is the major product within the spiran mechanism, and its relative yield is also generally higher compared to that of **AZ**. Only at high temperatures above 1500 K do the relative yields of **NP** and **AZ** become close. This may look surprising because the equilibrium of the **S4** → **S6** reaction is considerably shifted toward the **S6** adduct (K_{eq}(**S4** → **S6**) > 10^2 at $T < 1500$ K), which is an **AZ** precursor. To understand why **NP** production through the spiran pathway is much higher than that of **AZ**, one has to consider the competition between the **S4** → **S10** six-membered ring expansion, the **S6** → **S14** hydrogen-atom migration, and the reverse **S6** → **S4** step. The **S6** → **S14** reaction is crucial for the production of **AZ** because, as follows from the computed contributions to the total **AZ** yield shown in Table 1, the major **AZ** precursor is **S14**, whereas the contributions of the **S6** → **AZ** and **S13** → **AZ** hydrogen-

TABLE 2: RRKM- and TST-Calculated Rate Constants, Equilibrium Constants, and Their Ratios for Critical Reactions Involved in Rearrangements of 9HFLR at Temperatures Relevant to Combustion

	temperature, K							
rate constants	700	900	1000	1100	1300	1500	1700	2000
k(**S1** → **S2**), s^{-1}	1.8×10^{8}	1.4×10^{9}	2.9×10^{9}	5.2×10^{9}	1.3×10^{10}	2.6×10^{10}	4.3×10^{10}	7.7×10^{10}
k(**S2** → **S1**), s^{-1}	1.7×10^{12}	3.2×10^{12}	4.0×10^{12}	4.8×10^{12}	6.4×10^{12}	7.9×10^{12}	9.3×10^{12}	1.1×10^{13}
K_{eq}(**S1** → **S2**)	1.0×10^{-4}	4.4×10^{-4}	7.2×10^{-4}	1.1×10^{-3}	2.1×10^{-3}	3.3×10^{-3}	4.6×10^{-3}	6.9×10^{-3}
k(**S2** → **S3**), s^{-1}	$2.8 \times \times 10^{6}$	9.4×10^{7}	3.2×10^{8}	8.7×10^{8}	4.1×10^{9}	1.3×10^{10}	3.1×10^{10}	8.3×10^{10}
k(**S1** → **S26**), s^{-1}	7.6×10^{6}	2.0×10^{8}	6.3×10^{8}	1.6×10^{9}	7.2×10^{9}	2.1×10^{10}	4.9×10^{10}	1.3×10^{11}
k(**S26** → **S1**), s^{-1}	2.8×10^{3}	5.7×105	3.7×10^{6}	1.8×10^{7}	1.9×10^{8}	1.1×10^{9}	4.2×10^{9}	1.9×10^{10}
K_{eq}(**S1** → **S26**)	2.7×10^{3}	3.5×10^{2}	1.7×10^{2}	9.4×10^{1}	3.8×10^{1}	1.9×10^{1}	1.2×10^{1}	6.5
k(**S1** → **S2**)/k(**S1** → **S26**)	23.2	7.0	4.6	3.2	1.8	1.2	0.9	0.6
k(**S1** → **S26**)/k(**S2** → **S3**)	2.7	2.1	2.0	1.9	1.7	1.6	1.6	1.5
k(**S26** → **S32**), s^{-1}	1.9×10^{4}	2.2×10^{6}	1.2×10^{7}	4.7×10^{7}	3.9×10^{8}	1.9×10^{9}	6.2×10^{9}	2.4×10^{10}
k(**S26** → **FL**), s^{-1}	9.2×10^{-3}	6.0×10^{1}	1.3×10^{3}	1.7×10^{4}	8.4×10^{5}	1.5×10^{7}	1.4×10^{8}	1.7×10^{9}
k(**S32** → **FL**), s^{-1}	1.4×10^{-1}	5.1×10^{2}	9.1×10^{3}	9.9×10^{4}	3.9×10^{6}	5.8×10^{7}	4.6×10^{8}	4.8×10^{9}
k(**S6** → **S14**), s^{-1}	9.5×10^{5}	3.6×10^{7}	1.3×10^{8}	3.7×10^{8}	1.9×10^{9}	6.4×10^{9}	1.6×10^{10}	4.6×10^{10}
k(**S14** → **S6**), s^{-1}	4.4×10^{3}	5.6×10^{5}	3.1×10^{6}	1.3×10^{7}	1.1×10^{8}	5.3×10^{8}	1.8×10^{9}	7.2×10^{9}
K_{eq}(**S6** → **S14**)	2.2×10^{2}	6.4×10^{1}	4.2×10^{1}	2.9×10^{1}	1.7×10^{1}	1.2×10^{1}	8.9	6.4
k(**S6** → **S13**), s^{-1}	4.3×10^{1}	1.6×10^{4}	1.3×10^{5}	7.2×10^{5}	1.0×10^{7}	7.1×10^{7}	3.2×10^{8}	1.7×10^{9}
k(**S13** → **S6**), s^{-1}	3.0×10^{1}	1.2×10^{4}	9.6×10^{4}	5.4×10^{5}	7.7×10^{6}	5.5×10^{7}	2.5×10^{8}	1.4×10^{9}
K_{eq}(**S6** → **S13**)	1.42	1.36	1.36	1.34	1.29	1.29	1.27	1.25
k(**S4** → **S6**), s^{-1}	3.5×10^{12}	4.2×10^{12}	4.4×10^{12}	4.7×10^{12}	5.0×10^{12}	5.3×10^{12}	5.5×10^{12}	5.8×10^{12}
k(**S6** → **S4**), s^{-1}	1.4×10^{8}	1.4×10^{9}	3.2×10^{9}	6.3×10^{9}	1.8×10^{10}	3.8×10^{10}	6.8×10^{10}	1.3×10^{11}
K_{eq}(**S4** → **S6**)	2.5×10^{4}	3.0×10^{3}	1.4×10^{3}	7.5×10^{2}	2.8×10^{2}	1.4×10^{2}	8.1×10^{1}	4.5×10^{1}
k(**S4** → **S10**), s^{-1}	7.0×10^{8}	6.1×10^{9}	1.3×10^{10}	2.4×10^{10}	6.3×10^{10}	1.3×10^{11}	2.2×10^{11}	4.0×10^{11}
k(**S10** → **S4**), s^{-1}	2.4×10^{1}	1.1×10^{4}	9.8×10^{4}	5.8×10^{5}	8.8×10^{6}	6.6×10^{7}	3.0×10^{8}	1.7×10^{9}
K_{eq}(**S4** → **S10**)	2.9×10^{7}	5.6×10^{5}	1.3×10^{5}	4.1×10^{4}	7.2×10^{3}	2.0×10^{3}	7.2×10^{2}	2.4×10^{2}
k(**S4** → **S10**)/k(**S6** → **S14**)	738	168	99	64	33	20	13	9
k(**S6** → **S4**)/k(**S6** → **S14**)	146	39	25	17	9	6	4	2.8
k(**S3** → **S4**), s^{-1}	2.0×10^{8}	2.3×10^{9}	5.4×10^{9}	1.1×10^{10}	3.2×10^{10}	7.2×10^{10}	1.3×10^{11}	2.6×10^{11}
k(**S4** → **S3**), s^{-1}	5.2×10^{10}	1.8×10^{11}	2.7×10^{11}	3.9×10^{11}	6.7×10^{11}	1.0×10^{12}	1.4×10^{12}	1.9×10^{12}
K_{eq}(**S3** → **S4**)	3.9×10^{-3}	1.3×10^{-2}	2.0×10^{-2}	2.8×10^{-2}	4.8×10^{-2}	7.2×10^{-2}	9.7×10^{-2}	1.4×10^{-1}
k(**S3** → **S11**), s^{-1}	4.1×10^{5}	2.9×10^{7}	1.3×10^{8}	4.3×10^{8}	2.9×10^{9}	1.1×10^{10}	3.3×10^{10}	1.1×10^{11}
k(**S11** → **S3**), s^{-1}	1.3×10^{10}	3.3×10^{10}	4.7×10^{10}	6.1×10^{10}	9.2×10^{10}	1.3×10^{11}	1.6×10^{11}	2.1×10^{11}
K_{eq}(**S3** → **S11**)	3.2×10^{-5}	8.8×10^{-4}	2.8×10^{-3}	7.1×10^{-3}	3.2×10^{-2}	8.5×10^{-2}	2.1×10^{-1}	5.2×10^{-1}
k(**S3** → **S4**)/k(**S3** → **S11**)	488	80	42	25	11	6	4	2.4
k(**S6** → **S14**)/k(**S6** → **S13**)	22144	2246	1009	522	190	90	51	27
k(**AZ** + H → **S6**), $cm^3\ s^{-1}\ mol^{-1}$	2.4×10^{-13}	9.1×10^{-13}	1.5×10^{-12}	2.3×10^{-12}	4.4×10^{-12}	7.4×10^{-12}	1.1×10^{-11}	1.9×10^{-11}
k(**AZ** + H → **S13**), $cm^3\ s^{-1}\ mol^{-1}$	5.7×10^{-13}	2.0×10^{-12}	3.1×10^{-12}	4.6×10^{-12}	8.7×10^{-12}	1.4×10^{-11}	2.2×10^{-11}	3.5×10^{-11}
k(**AZ** + H → **S14**), $cm^3\ s^{-1}\ mol^{-1}$	3.4×10^{-12}	8.6×10^{-12}	1.2×10^{-11}	1.7×10^{-11}	2.7×10^{-11}	4.0×10^{-11}	5.5×10^{-11}	8.2×10^{-11}
k(**S1** → **S5**), s^{-1}	9.3×10^{2}	9.2×10^{4}	4.5×10^{5}	1.7×10^{6}	1.3×10^{7}	5.6×10^{7}	1.8×10^{8}	6.3×10^{8}
k(**S5** → **S1**), s^{-1}	1.6×10^{11}	4.6×10^{11}	6.6×10^{11}	8.9×10^{11}	1.4×10^{12}	2.0×10^{12}	2.6×10^{12}	3.5×10^{12}
K_{eq}(**S1** → **S5**)	5.8×10^{-9}	2.0×10^{-7}	6.9×10^{-7}	1.9×10^{-6}	9.0×10^{-6}	2.8×10^{-5}	6.7×10^{-5}	1.8×10^{-4}
k(**S1** → **S26**)/k(**S1** → **S5**)	8108	2182	1394	970	560	376	279	200
k(**S1** → **S2**)/k(**S1** → **S5**)	188518	15274	6376	3095	1026	455	246	122

elimination steps are insignificant. Although the equilibrium of the **S4** → **S6** seven-membered-ring expansion is shifted toward the formation of **S6**, the subsequent **S6** → **S14** H-migration is much slower than the competing reverse **S6** → **S4** and **S4** → **S10** steps. Indeed, if we look at the k(**S4** → **S10**)/k(**S6** → **S14**) ratios presented in Table 2, the **S4** → **S10** reaction is 738 times faster than **S6** → **S14** at 700 K, and it is still 20 times faster at 1500 K. On the other hand, as follows from the calculated k(**S6** → **S4**)/k(**S6** → **S14**) ratios, the **S6** → **S4** reverse step is also significantly faster than the **S6** → **S14** reaction by factors of 146, 25, 9, and 6 at 700, 1000, 1300, and 1500 K, respectively. Thus, once **S6** is formed, it tends to return back to the **S4** adduct, which then rapidly rearranges to **S10**. This explains, in general, why **NP** is the major product within the spiran mechanism. A decrease of the k(**S4** → **S10**)/k(**S6** → **S14**) and k(**S6** → **S4**)/k(**S6** → **S14**) ratios with increasing temperature also elucidates the growth of **AZ** production within the low-temperature regime (T < 1100 K). Indeed, when these ratios decrease, the **S14** production is favored, which is reflected in a rise of the total **AZ** yield. The relative contribution of **AZ** to the total **NP** + **AZ** production also increases within this temperature range, since the **NP** production is inhibited with increasing temperature by the competing **S1** → **S26** → **S32** → **FL** **FL**-formation channel. At T = 1100 K, the maximal production of **AZ** is observed, and then it starts to decrease as the temperature rises. This happens for two reasons. The first is that the total **NP** + **AZ** yield rapidly drops at T above 1100 K since the contending **FL** formation route starts to dominate; at 1500 K the **NP** + **AZ** production contributes only 12.7% to the overall final products. The second reason is that the relative contribution of the C−C bond scission mechanism (**S3** → **S11** → **S10** → **NP**) to the NP production increases with increasing temperature; for example, these contributions are 11%, 32%, and 48% at 700, 1100, and 1500 K, respectively. This means that the significant reduction of the spiran mechanism contribution to the total yield of **NP** and **AZ** is accompanied by an increasing relative contribution of the bond scission mechanism to the **NP** formation. Obviously, the bond scission mechanism competes

with the **S3** → **S4** ring closure, inhibiting the production of the **S4** adduct. Indeed, the calculated k(**S3** → **S4**)/k(**S3** → **S11**) ratio rapidly decreases when the temperature increases, from 488 at 700 K to 42 and 6 at 1000 and 1500 K, respectively. In other words, the **S3** → **S11** C−C bond-scission reaction acts as a sink of the spiro adduct **S3**, reducing the production of **S4**, which is the only **AZ** precursor within the spiran pathway.

The relative contribution of the bond-scission mechanism **S3** → **S11** → **S10** → **NP** to the **NP** yield is insignificant at low temperatures as compared to the **S3** → **S4** → **S10** → **NP** pathway involving the formation of tricyclyl intermediate **S4**. Here and below, we denote the later route as a "tricyclic" pathway; both the tricyclic and bond-scission routes are within the spiran mechanism, which proceeds via the formation of the spiro intermediate **S3**. The tricyclic pathway gives the major contribution to the **NP** production. However, when the temperature increases, the relative contribution of the bond-scission route rapidly increases and accounts for 26%, 40%, and 48% of the total **NP** yield at 1000, 1300, and 1500 K, respectively. At $T > 1500$ K, the bond scission route becomes the major **NP** formation pathway. The calculated k(**S3** → **S4**)/k(**S3** → **S11**) ratios shown in Table 2 rapidly decrease as the temperature rises, indicating that the competition between the **S3** → **S11** C−C bond scission and **S3** → **S4** ring-closure reactions increases. But even at 2000 K, the latter reaction is still 2.5 times faster than the former, and therefore it seems that the relative contribution of the tricyclic pathway to the **NP** yield should be higher than that from the bond scission route. However, the **S4** → **S10** ring-expansion step also competes with the very fast **S4** → **S6** reaction, which consumes some amount of the **S4** adduct to the **AZ** side; note that **AZ** accounts for ∼30% of the total **NP** + **AZ** yield at $T = 1500$ K and even more at higher temperatures. These facts explain the high relative contribution of the bond-scission mechanism to the **NP** production at medium and high temperatures, keeping in mind, of course, that **NP** becomes only a minor product in rearrangements of **S1** at these conditions.

Another **NP** formation route considered in the present study is the methylene walk pathway, **S13** → **S17** → **S22** → **S23** → **S24** → **NP**. According to the data presented in Table 1, the contributions of this mechanism to the **NP** yields are negligible at all studied temperatures. This is not surprising because the **S6** → **S14** hydrogen shift is significantly faster (by 3 orders of magnitude at 1000 K) than the competing **S6** → **S13** hydrogen migration, and it is still faster by a factor of 26 at 2000 K, as follows from the k(**S6** → **S14**)/k(**S6** → **S13**) ratios shown in Table 2. It is worth noting that the **AZ** production from the **S13** → **AZ** reaction is also negligible for the same reason. We may conclude that the methylene walk pathway does not play a significant role in rearrangements of **S1** with regard to the **NP** formation. However, this mechanism may be important if other **AZ** formation routes not necessarily related to the cyclopentadienyl recombination are considered. Indeed, if **AZ** is formed by another reaction pathway, for example, by sequential additions of acetylene and propargyl to c-C_5H_5, it may be activated by the hydrogen-addition reaction **AZ** + H → **S13**, and then **S13** can rearrange to **NP** by the methylene walk mechanism. The calculated bimolecular rate constants for the **AZ** + H → **S13**, **AZ** + H → **S14**, and **AZ** + H → **S6** hydrogen-addition reactions shown in Table 2 demonstrate similar values at medium and high temperatures, indicating that all three reactions are competitive at these conditions, and the formation of the **S13** adduct by H-addition may contribute to the **NP** formation via the methylene walk pathway. It can be seen from Table 1 that the highest contributions of the methylene walk mechanism to the **NP** yields correspond to the highest **AZ** production yields, indicating that an increase in the **AZ** concentration should result in higher **NP** production by the methylene walk channel.

In the previous section, we suggested an alternative rearrangement of the **S1** radical, **S1** → **S5** → **S6**, which proceeds via the formation of the tricyclic adduct **S5** to **S6**, and therefore may contribute to the **AZ** production. However, the calculated contributions of this pathway to the total **NP** + **AZ** yields appeared to be negligible at all studied temperatures. As follows from Table 2, the equilibrium constants for the **S1** → **S5** four-membered-ring closure step are very low within 700−2000 K; for instance, K_{eq}(**S1** → **S5**) < 10^{-3} even at $T = 2000$ K. Moreover, this reaction demonstrates significantly lower rate constants than the competitive **S1** → **S2** and **S1** → **S26** steps. In particular, the calculated k(**S1** → **S2**)/k(**S1** → **S5**) and k(**S1** → **S26**)/k(**S1** → **S5**) ratios shown in Table 2 indicate that the **S1** → **S2** rate constant is higher than that for the **S1** → **S5** step by 5−2 orders of magnitude within the 700−2000 K temperature interval, and the **S1** → **S26** hydrogen shift rate is also faster than k(**S1** → **S5**) by 3−2 orders of magnitude within the same temperature range. As a consequence, the **S1** → **S5** → **S6** rearrangement is not competitive with the spiran and **FL** pathways at the combustion conditions, and this mechanism can be safely excluded from consideration in kinetic modeling of flame combustion.

D. Implications for Kinetic Simulations. The results of our calculations of PESs for rearrangements of **S1** combined with RRKM calculations of rate constants and product yields predict the relative yields of **NP**, **FL**, and **AZ** at various combustion temperatures at the high-pressure limit. The computed contributions of different pathways to the final product yields help to qualitatively clarify the relative importance of each reaction channel in the production of these PAHs in both combustion and pyrolysis. Under real combustion conditions, however, the complete picture must be more complicated. The most important issue is that, in real systems, intermediate complexes or bimolecular products encounter numerous collisions, which can stabilize or destabilize them. In this case, the unimolecular or bimolecular reactions require a much more sophisticated theoretical description in terms of a time-dependent, multiple-well master equation (ME). By solving this equation, one can generate rate coefficients as a function of temperature and pressure, $k(T,p)$, which are required for modeling the macroscopic systems in combustion. The PES information for the reactions considered here will provide the raw data for the future RRKM/ME calculations of their temperature- and pressure-dependent rate constants, which can be further incorporated in the existing kinetic schemes for flame combustion to improve the prediction of PAH concentrations, especially those related to the cyclopentadienyl recombination. For the high-pressure limit, rate constants within the 300−3000 K temperature range computed with a 100 K step and given in Table S2 of the Supporting Information can be fit to various analytical expressions convenient for kinetic modeling.

In this section, we would like to discuss several issues, which may be important for and may affect the results of kinetic simulations of real combustion systems. First of all, to complete the picture, rearrangements on the $C_{10}H_{11}$ and $C_{10}H_{10}$ PES with regard to the formation of **NP**, **FL**, **AZ**, and, especially, indene, should be investigated. As was discussed above, the molecular−radical reactions of cyclopentadiene with the cyclopentadienyl radical (see Figure 1) may contribute to the production of the

PAHs considered in the present study. The *c*-C_5H_6 + *c*-C_5H_5 reaction produces **A1** (C_5H_6−C_5H_5), which may further be involved in rearrangements on the $C_{10}H_{11}$ PES leading to **NP**, **AZ**, and also indene. For instance, indene was identified as a major reaction product in the cyclopentadiene pyrolysis, and the mechanism accounting for the indene formation starting from the **A1** adduct was proposed.[10] As has been suggested by Carpenter, the formation of **NP** from the recombination of two cyclopentadienyl radicals may take place on the $C_{10}H_{10}$ PES by the isomerization of **S0** to 9,10-dihydronaphthalene. This pathway involves the formation of a tricyclic intermediate with a singlet biradical wave function, followed by ring-opening to a 10-membered cyclic structure, which finally rearranges to 9,10-dihydronaphthalene. **NP** can be produced from 9,10-dihydronaphthalene by the elimination of a H_2 molecule. This pathway should also be taken into consideration in a complete study of the reaction mechanisms from cyclic C_5 species to **NP**. However, the $C_{10}H_{11}$ and $C_{10}H_{10}$ rearrangements are beyond the scope of the present study and will be discussed in separate publications.

The second issue concerns the role of H radicals in the formation of PAH species. In our previous study of the HACA **NP** synthesis,[15] we suggested a bimolecular hydrogen disproportionation mechanism as an alternative to the commonly accepted unimolecular H-loss reaction for elimination of an "extra" hydrogen atom from PAH radicals such as **S6**, **S13**, **S14**, **S10**, **S24**, and **S26**. It is worth noting that elimination of such an "extra" hydrogen atom produces singlet PAH species (i.e., **NP**, **AZ**, **FL**, etc.). We suppose that, at high concentrations of free H radicals, the disproportionation mechanism may be favored over the direct H-loss considered for the **S6** → **AZ**, **S13** → **AZ**, **S14** → **AZ**, **S10** → **NP**, **S24** → **NP**, and **S26** → **FL** steps. According to our previous IRCMax{Energy-[G3(MP2,CC)]}//IRC{Geom[UMP2/6-31G*]} calculations, the barriers for the **S10** + H → **NP** + H_2 and 2-naphthyl + H → **NP** + H_2 disproportionation steps were found to be 1.2 kcal/mol and 2.3 kcal/mol, respectively.[15] These values are significantly lower than the respective barriers for the H-loss reactions **S10** → **NP** + H (14.8 kcal/mol) and 2-naphthyl → **NP** + H (27.8 kcal/mol). The hydrogen disproportionation reactions are also highly exothermic (by 80−100 kcal/mol), whereas the H-loss steps are usually strongly endothermic. Therefore, the hydrogen disproportionation mechanism may represent a viable alternative to the simple H-loss mechanism for the elimination of an extra hydrogen atom if the concentration of H radicals is sufficiently high. At this point, considering the disproportionation mechanism instead of the H-loss, we could expect different **NP**/**AZ** branching ratios within the spiran rearrangement. Indeed, if H-elimination from the **S6** intermediate occurs via the disproportionation mechanism **S6** + H → **AZ** + H_2, which is considerably faster than the **S6** → **AZ** + H reaction, the **S6** → **S4** → **S10** sequence may no longer be competitive, as compared to the case when only the direct H-loss mechanism is taken into account. This would result in higher **AZ** yields, which may then become the major reaction product within the spiran mechanism. On the other hand, at high H-radical concentrations, **AZ** may be activated by the hydrogen addition **AZ** + H → **S13**, followed by the rearrangement to **NP** through the methylene walk mechanism. As one can see, the consideration of H disproportionation considerably complicates the kinetics of the **S1** rearrangements. We suppose that the role of H radicals and the hydrogen disproportionation mechanism in particular required a separate investigation using kinetic simulations of real flame combustion with explicit consideration of H-radical concentrations. This can also help to better understand the role of the methylene walk pathway in the **AZ**-to-**NP** rearrangement, especially when some other **AZ** formation mechanisms can be realized.

4. Conclusions

Chemically accurate ab initio G3-type calculations of PESs for rearrangements of **S1** (C_5H_5−C_5H_4) have been performed, followed by RRKM computation of high-pressure-limit thermal rate constants and relative product yields. **NP**, **FL**, and **AZ** have been shown to be the reaction products, with relative yields depending on temperature. High **NP** yields have been calculated at low temperatures (T < 1000 K), where **NP** is inferred as the major reaction product. At T > 1000 K, the production of **NP** rapidly decreases with increasing temperature, whereas the production of **FL** increases, and the latter becomes the major reaction product. Starting from T = 1500 K, **NP** becomes only a minor product accounting for, together with **AZ**, less than 10% of the total reaction yield. The computed branching ratios demonstrate that the cyclopentadienyl radical recombination is not likely to be a significant source of **NP** in combustion flames at medium and high temperatures and at the high-pressure limit. More likely, in this case, the common HACA mechanism gives the major contribution to the **NP** formation. In contrast, at a low-temperature pyrolytic regime, the contribution of the **S1** rearrangements to the **NP** production is expected to be high, which is in agreement with experimental observations in the cyclopentadiene pyrolysis.[10,26] **AZ** has been found only as a minor product, and its branching ratio does not exceed 5% at all studied temperatures. Since FL is predicted to be the major product at T > 1000 K, the cyclopentadienyl recombination is more likely to be a significant source of various cyclopentafused PAHs (possible fullerene precursors) at medium and high combustion temperatures.

The spiran pathway originally suggested by Melius et al.[3] has been shown as the major contributor to the **NP** production at low combustion temperatures (T < 1000 K). The alternative C−C bond scission route, which proceeds via the formation of the **S11** radical, becomes important only at higher temperatures, where the total **NP** yields are low. The contributions of the previously suggested methylene walk pathway[9] to the production of **NP** is found to be negligible at all temperatures relevant to combustion; however, this route may be important if **AZ** is produced by different mechanisms.

Our RRKM-computed rate constants for the considered **S1** rearrangement pathways are expected to be of high accuracy for the conditions where the high-pressure limit is adequate, and they can be included in the existing kinetic schemes for modeling of flame combustion to improve the prediction of various PAHs (especially, **NP**, **AZ**, **FL**, and cyclopentafused PAH) and their concentration profiles.

Acknowledgment. This work is funded by the Chemical Sciences, Geosciences and Biosciences Division, Office of Basic Energy Sciences, Office of Sciences of the U.S. Department of Energy (Grant No. DE-FG02-04ER15570).

Supporting Information Available: Calculated total energies at the B3LYP, CCSD(T), MP2, and G3 levels of theory, ZPE corrections, vibrational frequencies, moments of inertia, rotational constants, and optimized Cartesian coordinates of all species involved in the studied mechanisms (Table S1); RRKM- and TST-calculated high-pressure-limit thermal rate constants for all studied reactions within the 300−3000 K temperature

range (Table S2). This material is available free of charge via the Internet at http://pubs.acs.org.

References and Notes

(1) Richter, H.; Howard, J. B. *Prog. Energy Combust. Sci.* **2000**, *26*, 565.

(2) Miller, J. A.; Melius, C. F. *Combust. Flame* **1992**, *91*, 21.

(3) Melius, C. F.; Colvin, M. E.; Marinov, N. M.; Pitz, W. J.; Senkan, S. M. *Proc. Int. Symp. Combust.* **1996**, *26*, 685.

(4) Moskaleva, L. V.; Mebel, A. M.; Lin, M. C. *Proc. Int. Symp. Combust.* **1996**, *26*, 521.

(5) Marinov, N. M.; Pitz, W. J.; Westbrook, C. K.; Vincitore, A. M.; Castaldi, M. J.; Senkan, S. M.; Melius, C. F. *Combust. Flame* **1998**, *114*, 192.

(6) Castaldi, M. J.; Marinov, N. M.; Melius, C. F.; Huang, J.; Senkan, S. M.; Pitz, W. J.; Westbrook, C. K. *Proc. Int. Symp. Combust.* **1996**, *26*, 693.

(7) Hansen, N.; Klippenstein, S. J.; Miller, J. A.; Wang, J.; Cool, T. A.; Law, M. E.; Westmoreland, P. R.; Kasper, T.; Kohse-Hoinghaus, K. *J. Phys. Chem. A* **2006**, *110*, 4376.

(8) Frenklach, M.; Wang, H. *Proc. Combust. Inst.* **1991**, *23*, 1559.

(9) Alder, R. W.; East, S. P.; Harvey, J. N.; Oakley, M. T. *J. Am. Chem. Soc.* **2003**, *125*, 5375.

(10) Wang, D.; Violi, A.; Kim, D. H.; Mullholland, J. A. *J. Phys. Chem. A* **2006**, *110*, 4719.

(11) Dyakov, Y. A.; Ni, C.-K.; Lin, S. H.; Lee, Y. T.; Mebel, A. M. *J. Phys. Chem. A* **2005**, *109*, 8774.

(12) (a) Becke, A. D. *J. Chem. Phys.* **1992**, *96*, 2155. (b) Becke, A. D. *J. Chem. Phys.* **1992**, *97*, 9173. (c) Becke, A. D. *J. Chem. Phys.* **1993**, *98*, 5648. (d) Lee, C.; Yang, W.; Parr, R. G. *Phys. Rev.* **1988**, *B37*, 785.

(13) (a) Baboul, A. G.; Curtiss, L. A.; Redfern, P. C.; Raghavachari, K. *J. Chem. Phys.* **1999**, *110*, 7650. (b) Curtiss, L. A.; Raghavachari, K.; Redfern, P. C.; Baboul, A. G.; Pople, J. A. *Chem. Phys. Lett.* **1999**, *314*, 101.

(14) Curtiss, L. A.; Raghavachari, K.; Redfern, P. C.; Rassolov, V.; Pople, J. A. *J. Chem. Phys.* **1998**, *109*, 7764.

(15) Kislov, V. V.; Islamova, N. I.; Kolker, A. M.; Lin, S. H.; Mebel, A. M. *J. Chem. Theory Comput.* **2005**, *1*, 908.

(16) Kislov, V. V.; Mebel, A. M. *J. Phys. Chem. A* **2007**, *111*, 3922.

(17) Frisch, M. J.; Trucks, G. W.; Schlegel, H. B.; Scuseria, G. E.; Robb, M. A.; Cheeseman, J. R.; Zakrzewski, V. G.; Montgomery, J. A.; Stratmann, R. E.; Burant, J. C.; Dapprich, S.; Millam, J. M.; Daniels, R. E.; Kudin, K. N.; Strain, M. C.; Farkas, O.; Tomasi, J.; Barone, V.; Cossi, M.; Cammi, R.; Mennucci, B.; Pomelli, C.; Adamo, C.; Clifford, S.; Ochterski, J.; Petersson, G. A.; Ayala, P. Y.; Cui, Q.; Morokuma, K.; Salvador, P.; Dannenberg, J. J.; Malick, D. K.; Rabuck, A. D.; Raghavachari, K.; Foresman, J. B.; Cioslowski, J.; Ortiz, J. V.; Baboul, A. G.; Stefanov, B. B.; Liu, G.; Liashenko, A.; Piskorz, P.; Komaromi, I.; Gomperts, R.; Martin, R. L.; Fox, D. J.; Keith, T.; Al-Laham, M. A.; Peng, C. Y.; Nanayakkara, A.; Challacombe, M.; Gill, P. M. W.; Johnson, B.; Chen, W.; Wong, M. W.; Andres, J. L.; Gonzalez, C.; M. Head-Gordon, M.; Replogle, E. S.; Pople, J. A. *Gaussian 98*, revision A.11; Gaussian, Inc.: Pittsburgh, PA, 2001.

(18) Amos, R. D.; Bernhardsson, A.; Berning, A.; Celani, P.; Cooper, D. L.; Deegan, M. J. O.; Dobbyn, A. J.; Eckert, F.; Hampel, C.; Hetzer, G.; Knowles, P. J.; Korona, T.; Lindh, R.; Lloyd, A. W.; McNicholas, S. J.; Manby, F. R.; Meyer, W.; Mura, M. E.; Nicklass, A.; Palmieri, P.; Pitzer, R.; Rauhut, G.; Schutz, M.; Schumann, U.; Stoll, H.; Stone, A. J.; Tarroni, R.; Thorsteinsson, T.; Werner, H.-J. *MOLPRO*, version 2002.1; MOLPRO is a package of ab initio programs designed by H. J. Werner and P. J. Knowles. http://www.molpro.net.

(19) Steinfield, J.; Francisco, J.; Hase, W. *Chemical Kinetics and Dynamics*; Prentice Hall: Englewood Cliffs, NJ, 1989.

(20) Eyring, H.; Lin, S. H.; Lin, S. M. *Basic Chemical Kinetics*; Wiley: New York, 1980.

(21) Robinson, P. J.; Holbrook, K. A. *Unimolecular Reactions*; Wiley: New York, 1972.

(22) Glasstone, S.; Laidler, K. J.; Eyring, H. *The Theory of Rate Processes*; McGraw-Hill: New York, 1941.

(23) Press, W. H.; Teukolsky, S. A.; Vetterling, W. T., Flannery, B. P. *Numerical Recipes in Fortran 77: The Art of Scientific Computing*, 2nd ed.; Cambridge University Press: Cambridge, U.K., 1992.

(24) Scott, L. T.; Cheng, P.-C.; Hashemi, M. M.; Bratcher, M. S.; Meyer, D. T.; Warren, H. B. *J. Am. Chem. Soc.* **1997**, *119*, 10963.

(25) Cioslowski, J.; Schimeczek, M.; Piskorz, P.; Moncrieff, D. *J. Am. Chem. Soc.* **1999**, *121*, 3773.

(26) Lu, M.; Mulholland, J. A. *Chemosphere* **2004**, *55*, 605.

(27) Tokmakov, I. V.; Kim, G. S.; Kislov, V. V.; Mebel, A. M.; Lin, M. C. *J. Phys. Chem. A* **2005**, *109*, 6114.

(28) Dupont, L.; El Bakali, A.; Pauwels, J. F.; Da Costa, I.; Meunier, P.; Richter, H. *Combust. Flame* **2003**, *135*, 171.